Current Biology

A Neanderthal Sodium Channel Increases Pain Sensitivity in Present-Day Humans

Highlights

- Some present-day humans carry a Neanderthal variant of the sodium channel Nav1.7

- The Neanderthal variant carries three amino acid differences to the common variant

- The Neanderthal channel is more likely to be in a ready-to-open state

- Carriers of the Neanderthal variant experience more pain

Authors

Hugo Zeberg, Michael Dannemann, Kristoffer Sahlholm, ...,
Hugh P.C. Robinson, Janet Kelso,
Svante Pääbo

Correspondence

hugo.zeberg@ki.se (H.Z.),
paabo@eva.mpg.de (S.P.)

In Brief

Zeberg et al. show that a Neanderthal variant of the sodium channel Nav1.7, which is crucial for the initiation of the pain signals, occurs in some humans today. The Neanderthal variant differs from the common variant in its electrophysiological properties and is associated with increased sensitivity to pain.

CellPress

Current Biology

Report

A Neanderthal Sodium Channel Increases Pain Sensitivity in Present-Day Humans

Hugo Zeberg,[1,2,6,*] Michael Dannemann,[1] Kristoffer Sahlholm,[2,3] Kristin Tsuo,[1] Tomislav Maricic,[1] Victor Wiebe,[1] Wulf Hevers,[1] Hugh P.C. Robinson,[2,4] Janet Kelso,[1] and Svante Pääbo[1,5,*]

[1]Max Planck Institute for Evolutionary Anthropology, Deutscher Platz 6, 04103 Leipzig, Germany
[2]Department of Neuroscience, Karolinska Institutet, 17177 Stockholm, Sweden
[3]Department of Integrative Medical Biology, Wallenberg Centre for Molecular Medicine, Umeå University, 90187 Umeå, Sweden
[4]Department of Physiology, Development and Neuroscience, University of Cambridge, Cambridge CB2 3EG, UK
[5]Okinawa Institute of Science and Technology, Onna-son, Okinawa 904-0495, Japan
[6]Lead Contact
*Correspondence: hugo.zeberg@ki.se (H.Z.), paabo@eva.mpg.de (S.P.)
https://doi.org/10.1016/j.cub.2020.06.045

SUMMARY

The sodium channel Nav1.7 is crucial for impulse generation and conduction in peripheral pain pathways [1]. In Neanderthals, the Nav1.7 protein carried three amino acid substitutions (M932L, V991L, and D1908G) relative to modern humans. We expressed Nav1.7 proteins carrying all combinations of these substitutions and studied their electrophysiological effects. Whereas the single amino acid substitutions do not affect the function of the ion channel, the full Neanderthal variant carrying all three substitutions, as well as the combination of V991L with D1908G, shows reduced inactivation, suggesting that peripheral nerves were more sensitive to painful stimuli in Neanderthals than in modern humans. We show that, due to gene flow from Neanderthals, the three Neanderthal substitutions are found in ~0.4% of present-day Britons, where they are associated with heightened pain sensitivity.

RESULTS AND DISCUSSION

Neanderthals and their Asian relatives, Denisovans, evolved largely separately from the ancestors of present-day humans for about 500,000 years [2]. During that time, each group independently accumulated genetic changes that became frequent or fixed. However, late in their history, Neanderthals and Denisovans mixed with modern humans, which resulted in many genetic variants from Neanderthals and Denisovans being present in humans today [3, 4]. As several Neanderthal genomes of high quality are now available [2, 5, 6], it is possible to identify genetic changes that occurred in many or most Neanderthals, investigate their physiological effects, and assess their consequences when they occur in people today.

Whereas most genetic differences between Neanderthals and modern humans that affect gene products occur singly in genes across the genome, genes that carry several such differences are of particular note. One such case is the gene *SCN9A*, which encodes the Nav1.7 protein, a voltage-gated sodium channel in which all Neanderthal genomes sequenced to date carry three amino acid substitutions relative to modern humans: M932L; V991L; and D1908G. At these positions, extant monkeys and apes share the modern human residues. Nav1.7 is the only ion channel carrying amino acid substitutions in Neanderthals that is highly expressed in peripheral nerves mediating pain sensation [7]. The channel allows for the passage of sodium ions across the membranes of neurons in response to changes in electrical membrane potential. In humans, loss-of-function mutations of *SCN9A* cause insensitivity to pain [8] and anosmia

[9]. Gain-of-function mutations, on the other hand, are a leading cause of idiopathic small-fiber neuropathy [1], where patients present with sensory symptoms and pain, with pain as the dominant symptom [10].

To investigate the electrophysiological effects of the three substitutions seen in Neanderthals, we synthesized genes encoding the modern human and Neanderthal versions of Nav1.7, transcribed these *in vitro*, and injected the mRNAs into *Xenopus laevis* oocytes. We chose this system, rather than, for example, cultured murine dorsal root ganglion cells, in order to test the effects of the three amino acid substitutions when expressed together with relevant human subunits, which differ from those of rodents by 5–47 amino acids. In peripheral nerve endings, Nav1.7 forms complexes with the β3 subunit [11–13], encoded by *SCN3B*, which carries no amino acid differences between Neanderthals, Denisovans, and modern humans. When the β3 subunit is expressed together with Nav1.7 in the oocytes, the inactivation curve of the Neanderthal ion channel is shifted by ~6.1 mV toward less negative values relative to the modern human channel (Figures 1A and 1B; Table S1; $p = 2.9 \times 10^{-5}$; n = 26 and n = 31, respectively). This results in an increased availability of sodium channels for activation and increased probability that the sodium channel remains open for a longer time once activated and is expected to lower the threshold for the generation of an action potential (see computational model; Figures S1M and S1N).

To examine which of the amino acid substitutions mediates the shift in the inactivation curve, we synthesized and injected mRNAs encoding each of the three amino acid substitutions
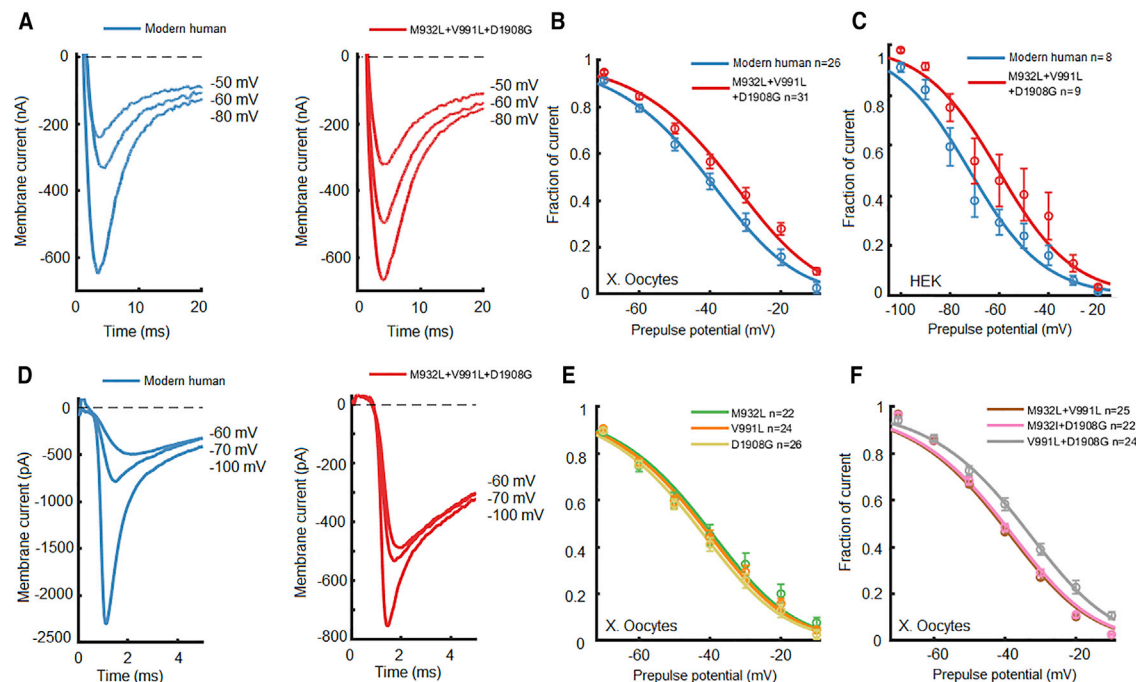
Figure 1. Effects of Neanderthal-Derived Amino Acid Substitutions on Nav1.7 Inactivation

(A) Current traces from *Xenopus laevis* oocytes expressing modern human and Neanderthal (M932L+V991L+D1908G) Nav1.7 proteins together with the auxiliary subunit Navβ3. Following prepulses to three different potentials (shown as examples), currents were elicited by stepping to 0 mV (t = 0). Less negative prepulse potentials resulted in progressively smaller currents due to channel inactivation. This inactivation is more pronounced for the modern human than the Neanderthal protein.

(B) Fraction of current as a function of prepulse potential for the modern human and Neanderthal channel proteins. Current amplitudes, measured at t = 10 ms, were normalized to the largest amplitude obtained in each cell. The voltage required for half-maximal inactivation is shifted by +6.1 mV for the Neanderthal protein.

(C) Fraction of current as a function of prepulse potential for the modern human and Neanderthal channel proteins when expressed in human embryonic kidney (HEK) cells. Current amplitudes, measured as peak inward current, were normalized to the largest amplitude obtained in each cell. The voltage required for half-maximal inactivation is shifted by +11.7 mV for the Neanderthal protein.

(D) Current traces from HEK cells expressing modern human and Neanderthal (M932L+V991L+D1908G) Nav1.7 proteins together with the auxiliary subunit Navβ3

(E) Fraction of current as a function of prepulse potential in *Xenopus* oocytes for the three single amino acid substitutions individually.

(F) Fraction of current in *Xenopus* oocytes as a function of prepulse potential for Nav1.7 proteins with two substitutions. The voltage required for half-maximal inactivation is shifted by +6.2 mV for the V991L+D1908G protein. Compared to mammalian cells, the steady-state inactivation curves are shifted to the right due to the recording temperature (10°C ± 2°C), the co-expression of the β3 subunit, and the use of *Xenopus* oocytes, as described [14–16].

Error bars represent SEM. See also Figures S1 and S2 and Table S1.

singly (Figure S2). No single amino acid substitution had any effect on the inactivation of the ion channel (Figure 1E; Table S1). We next investigated the effect of the three possible combinations of two amino acid substitutions. Two of the combinations, M932L+D1908G and M932L+V991L, had no effect on the inactivation. However, V991L+ D1908G caused a shift in the inactivation curve, similar to that of the three substitutions (Figure 1F; Table S1; p = 2.4 × 10^{-5}; n = 24). Thus, an epistatic interaction of the two substitutions V991L and D1908G, which are both located in the intracellular part of the protein, is necessary to elicit the electrophysiological effects. In contrast, M932L, which is located extracellularly, had no detectable effects. We note that the Denisovan genome carries the D1908G substitution in a homozygous form but lacks the other two substitutions. This suggests that the D1908G substitution occurred in the common ancestor of Neanderthals and Denisovans but that it may

have had a functional effect only in Neanderthals, where also the V991L substitution occurred.

To test whether the effects of the Neanderthal substitutions are also seen in mammalian cells, we transfected human embryonic kidney (HEK) cells with vectors expressing the mRNAs encoding the modern human and the Neanderthal variants of Nav1.7 and the β3 subunit. As in the oocytes, we observe a depolarizing shift in inactivation for the Neanderthal variant of Nav1.7 (Figure 1C; Table S1; p = 9.1 × 10^{-3}; n = 8 and n = 9, respectively). In addition, we observe a depolarizing shift of the activation curve (Figure S1C; Table S1; p = 1.1 × 10^{-3}; n = 8 and n = 9, respectively). When investigated in a simple model of a human peripheral nerve, the depolarizing shift in the inactivation curve has an excitatory effect for suprathreshold stimuli, even in the presence of a depolarizing shift in activation (Figure S1N). Thus, we conclude that the shifts seen in both oocytes and HEK cells are likely to have an excitatory action.
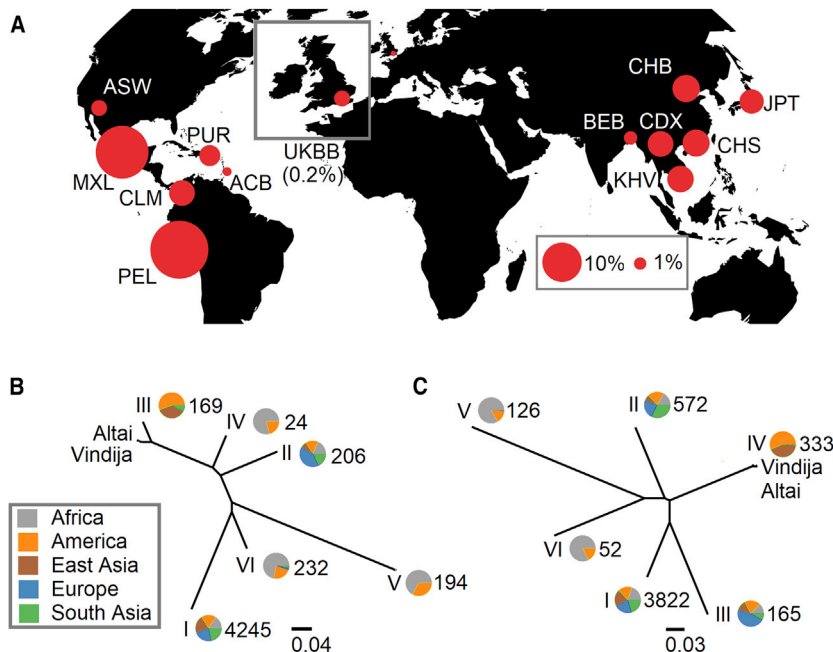
Current Biology
Report

Figure 2. Geographical Distribution and Phylogenetic Relationships of *SCN9A* Variants

(A) Allele frequencies of the variant with all amino acid substitutions (M932L+V991L+D1908G) in 1000G populations and in the UK Biobank (0.2%, inset).

(B and C) Phylogenetic relationship between modern human DNA sequences and the corresponding genome sequences of two Neanderthals in the two genomic regions encompassing (B) M932L (rs12478318) and V991L (rs4369876), and (C) D1908G (rs3750904) are shown as unrooted maximum likelihood trees. Roman numerals indicate clusters of closely related DNA sequences, and their geographical distribution is shown as pie charts. For both genomic regions, one group of modern human DNA sequences is most closely related to the Neanderthal genome sequences (B: cluster III; C: cluster IV). Altai and Vindija are archaeological sites, here denoting one Neanderthal DNA sequence from each site [2, 6].

See also Table S2.

We next investigated whether any of the three *SCN9A* missense mutations (M932L, V991L, and D1908G) exist in present-day humans by examining 2,535 genomes available in the phase III 1000 Genomes (1000G) dataset (Figure 2A). We did not find any of the three variants in the African (N = 507) and European (N = 505) 1000G populations, but M932L and V991L occur in almost perfect linkage disequilibrium (R^2 = 0.99) at frequencies of 0.9%–7.8% in Asia and 0.5%–23.8% in the Americas. In addition, D1908G occurs at a frequency of 0%–17.1% in Asia and 0.5%–52.9% in the Americas (Table S2) and tends to be in linkage disequilibrium with M932L+V991L (R^2 = 0.26).

These variants could have entered the present-day human population from a common ancestor shared with Neanderthals and Denisovans or by introgression from archaic hominins when these met modern humans some 40,000–60,000 years ago. In the latter case, the size of the archaic-like DNA segments on which the variants sit are expected to be substantially larger than if they were inherited from a common ancestor of the three groups, as meiotic recombination will have had less time to reduce their size. To estimate the size of these segments, we identified alleles in this genomic region that are absent in the 1000G Yoruba individuals but occur in homozygous form in the Neanderthal and/or Denisovan genomes and are likely to have entered modern human populations from archaic hominins. We identified one DNA segment (r^2 > 0.8) of ~26 kb around the M932L and V991L substitutions carrying 14 such alleles (chr2:167129256–167155131) and another segment (r^2 > 0.8) of ~110 kb around the D1908G substitution carrying 40 such alleles (chr2:167017315–167126999).

Based on the sizes of the two DNA segments and their recombination rates, we concluded that these variants entered the modern human population by introgression from Neanderthals or Denisovans, rather than being inherited from a common ancestor of the groups (p = 0.059 for V991L and M932L; p = 7.8 × 10^{-16} for D1908G). We estimated the phylogenetic

relationships of the two DNA segments overlapping M932L+V991L and D1908G to the corresponding present-day human and Neanderthal DNA segments. For both segments, one group of present-day human DNA sequences is most closely related to the Neanderthal segments (Figures 2B and 2C), and in both instances, these DNA sequences are found in Asia and the Americas.

The amino acid substitutions M932L and V991L have previously been associated with increased pain sensitivity and small-fiber neuropathy in experimental and clinical studies in humans [1, 17]. To investigate whether the three introgressed Neanderthal variants affect pain sensitivity in the general human population, we selected 362,944 unrelated individuals of British ancestry in the UK Biobank (UKBB) [18] who had answered questions relating to their experience of pain (Table S3). Although no individual was homozygous for the Neanderthal variants, 1,327 individuals (0.4%) carried all three amino acid substitutions in a heterozygous form. Based on their answers to 19 pain-related questions, these carriers of the three Neanderthal substitutions had experienced one or more forms of pain more often than non-carriers (Figure 3; p = 0.0078; adjusted for age and sex). They also experienced more pain than carriers of only one or two of the Neanderthal substitutions, although these did not differ significantly from individuals carrying none of the Neanderthal substitutions (Figure 3). No individuals with the combination V991L and D1908G were found in the UKBB. Two other substitutions in Nav1.7 that have previously been reported to be associated with increased pain sensitivity are also genotyped in the UKBB and frequent enough to assess their phenotype (W1150R, n = 91,143; R185H, n = 1,369). Neither of these are associated with an increased probability to report pain (p = 0.82 and p = 0.72, respectively), suggesting that their effects are smaller than the Neanderthal-derived variants.

Notably, sex did not affect the extent to which individuals in the UKBB report pain (p = 0.84; 198,047 females; 164,897 males),
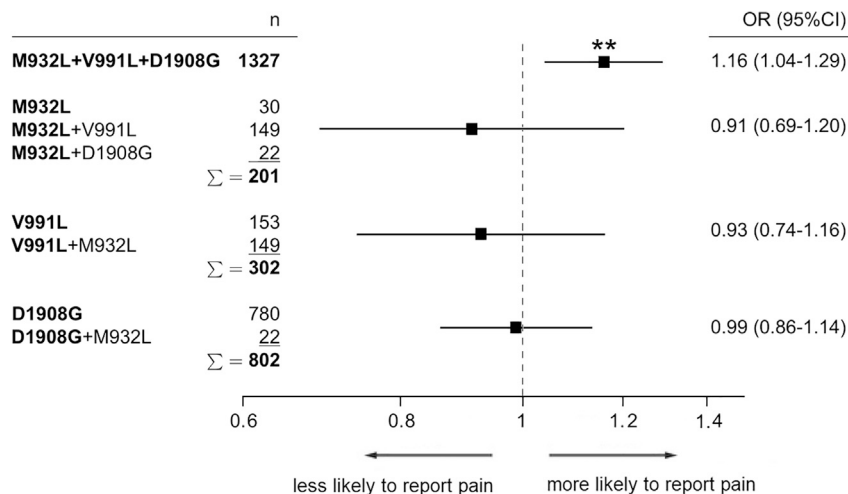
Figure 3. Pain Sensitivity among UK Biobank Individuals (n = 362,944)
Odds ratios (ORs) for reporting pain among individuals carrying all three amino acid substitutions (M932L+V991L+D1908G) and for each amino acid substitution singly or in a combination with one other substitution (but not all three) relative to the rest of the UKBB individuals. No individual carried V991L+D1908G. The low frequencies of the three individual variants of M932L: 0.21%, V991L: 0.23%, and D1908G: 0.29% are consistent with observations in the 1000G (0 of 100 in England and Scotland; Table S2). Horizontal lines indicate 95% confidence intervals. See also Figure S3 and Table S3.

whereas age showed an approximately linear and positive correlation with reported pain between the ages of 40 and 70 (Figure S3; p = 4.6 × 10^{-282}). Individuals who carried the three amino acid substitutions inherited from Neanderthals in heterozygous form are 7% more likely to report at least one form of pain compared to people without these substitutions. This corresponds to an increase of approximately 8.5 years in terms of pain reported. At the present time, we can only speculate about the consequences of having these substitutions in homozygous form, as was the case in the three Neanderthals genomes have been sequenced to high coverage.

We note that Nav1.7 is expressed also in other cell types, for example, olfactory neurons, raising the possibility that the substitutions studied here might have additional effects beyond modulation of pain. However, given the electrophysiological effects of the substitutions, nociception, i.e., the input to the central nervous system from peripheral nerves in response to harmful or potentially harmful stimuli, is likely to have been higher in Neanderthals than in modern humans. The translation of such input into the conscious perception of pain is modulated both at the level of the spinal cord and the brain. Thus, it is not possible to conclude that Neanderthals necessarily experienced more pain than modern humans do. Yet the input from Neanderthal peripheral nerve endings would have allowed Neanderthals to be more sensitive to stimuli, as suggested by the observations in present-day people heterozygous for the Neanderthal Nav1.7 variant.

STAR★METHODS

Detailed methods are provided in the online version of this paper and include the following:

- KEY RESOURCES TABLE
- RESOURCE AVAILABILITY
  - Lead Contact
  - Materials Availability
  - Data and Code Availability
- EXPERIMENTAL MODEL AND SUBJECT DETAILS
- METHOD DETAILS
  - Molecular biology
  - Oocyte injection
  - Transfection of HEK293T cells
  - Voltage clamp recordings in *Xenopus* oocytes
  - Voltage clamp experiments in HEK293T cells
  - Computational modeling
  - Amino-acid substitutions in Neanderthal ion channels
  - Archaic introgression
  - Phenotypic consequences of Nav1.7 variants
- QUANTIFICATION AND STATISTICAL ANALYSIS
- ADDITIONAL RESOURCES

SUPPLEMENTAL INFORMATION

Supplemental Information can be found online at https://doi.org/10.1016/j.cub.2020.06.045.

AUTHOR CONTRIBUTIONS

H.Z., M.D., J.K., and S.P. designed the study; H.Z. performed the electrophysiological experiments with assistance from K.S., H.P.C.R., and W.H. M.D., K.T., J.K., and S.P. did phylogenetic analyses; M.D. and H.Z. studied the phenotypic effects in UKBB; V.W. performed the *in vitro* translation; and H.Z., M.D., and S.P. wrote the manuscript with input from all authors.

DECLARATION OF INTERESTS

The authors declare no competing interests.

REFERENCES

1. Dib-Hajj, S.D., Yang, Y., Black, J.A., and Waxman, S.G. (2013). The Na(V) 1.7 sodium channel: from molecule to man. Nat. Rev. Neurosci. *14*, 49–62.

Current Biology
Report

2. Prüfer, K., Racimo, F., Patterson, N., Jay, F., Sankararaman, S., Sawyer, S., Heinze, A., Renaud, G., Sudmant, P.H., de Filippo, C., et al. (2014). The complete genome sequence of a Neanderthal from the Altai Mountains. Nature *505*, 43–49.

3. Sankararaman, S., Patterson, N., Li, H., Pääbo, S., and Reich, D. (2012). The date of interbreeding between Neandertals and modern humans. PLoS Genet. *8*, e1002947.

4. Vernot, B., Tucci, S., Kelso, J., Schraiber, J.G., Wolf, A.B., Gittelman, R.M., Dannemann, M., Grote, S., McCoy, R.C., Norton, H., et al. (2016). Excavating Neandertal and Denisovan DNA from the genomes of Melanesian individuals. Science *352*, 235–239.

5. Hajdinjak, M., Fu, Q., Hübner, A., Petr, M., Mafessoni, F., Grote, S., Skoglund, P., Narasimham, V., Rougier, H., Crevecoeur, I., et al. (2018). Reconstructing the genetic history of late Neanderthals. Nature *555*, 652–656.

6. Prüfer, K., de Filippo, C., Grote, S., Mafessoni, F., Korlević, P., Hajdinjak, M., Vernot, B., Skov, L., Hsieh, P., Peyrégne, S., et al. (2017). A high-coverage Neandertal genome from Vindija Cave in Croatia. Science *358*, 655–658.

7. Usoskin, D., Furlan, A., Islam, S., Abdo, H., Lönnerberg, P., Lou, D., Hjerling-Leffler, J., Haeggström, J., Kharchenko, O., Kharchenko, P.V., et al. (2015). Unbiased classification of sensory neuron types by large-scale single-cell RNA sequencing. Nat. Neurosci. *18*, 145–153.

8. Cox, J.J., Reimann, F., Nicholas, A.K., Thornton, G., Roberts, E., Springell, K., Karbani, G., Jafri, H., Mannan, J., Raashid, Y., et al. (2006). An SCN9A channelopathy causes congenital inability to experience pain. Nature *444*, 894–898.

9. Weiss, J., Pyrski, M., Jacobi, E., Bufe, B., Willnecker, V., Schick, B., Zizzari, P., Gossage, S.J., Greer, C.A., Leinders-Zufall, T., et al. (2011). Loss-of-function mutations in sodium channel Nav1.7 cause anosmia. Nature *472*, 186–190.

10. Devigili, G., Tugnoli, V., Penza, P., Camozzi, F., Lombardi, R., Melli, G., Broglio, L., Granieri, E., and Lauria, G. (2008). The diagnostic criteria for small fibre neuropathy: from symptoms to neuropathology. Brain *131*, 1912–1925.

11. Ho, C., Zhao, J., Malinowski, S., Chahine, M., and O'Leary, M.E. (2012). Differential expression of sodium channel β subunits in dorsal root ganglion sensory neurons. J. Biol. Chem. *287*, 15044–15053.

12. Kanellopoulos, A.H., Koenig, J., Huang, H., Pyrski, M., Millet, Q., Lolignier, S., Morohashi, T., Gossage, S.J., Jay, M., Linley, J.E., et al. (2018). Mapping protein interactions of sodium channel Nav1.7 using epitope-tagged gene-targeted mice. EMBO J. *37*, 427–445.

13. Barro-Soria, R., Liin, S.I., and Larsson, H.P. (2017). Using fluorescence to understand β subunit-Nav channel interactions. J. Gen. Physiol. *149*, 757–762.

14. Maertens, C., Cuypers, E., Amininasab, M., Jalali, A., Vatanpour, H., and Tytgat, J. (2006). Potent modulation of the voltage-gated sodium channel Nav1.7 by OD1, a toxin from the scorpion Odonthobuthus doriae. Mol. Pharmacol. *70*, 405–414.

15. Han, C., Lampert, A., Rush, A.M., Dib-Hajj, S.D., Wang, X., Yang, Y., and Waxman, S.G. (2007). Temperature dependence of erythromelalgia mutation L858F in sodium channel Nav1.7. Mol. Pain *3*, 3.

16. Dib-Hajj, S.D., Choi, J.S., Macala, L.J., Tyrrell, L., Black, J.A., Cummins, T.R., and Waxman, S.G. (2009). Transfection of rat or mouse neurons by biolistics or electroporation. Nat. Protoc. *4*, 1118–1126.

17. Li, Q.S., Cheng, P., Favis, R., Wickenden, A., Romano, G., and Wang, H. (2015). SCN9A variants may be implicated in neuropathic pain associated with diabetic peripheral neuropathy and pain severity. Clin. J. Pain *31*, 976–982.

18. Sudlow, C., Gallacher, J., Allen, N., Beral, V., Burton, P., Danesh, J., Downey, P., Elliott, P., Green, J., Landray, M., et al. (2015). UK biobank: an open access resource for identifying the causes of a wide range of complex diseases of middle and old age. PLoS Med. *12*, e1001779.

19. Jespersen, T., Grunnet, M., Angelo, K., Klaerke, D.A., and Olesen, S.P. (2002). Dual-function vector for protein expression in both mammalian cells and Xenopus laevis oocytes. Biotechniques *32*, 536–538, 540.

20. Frankenhaeuser, B., and Moore, L.E. (1963). The effect of temperature on the sodium and potassium permeability changes in myelinated nerve fibres of Xenopus laevis. J. Physiol. *169*, 431–437.

21. Kusano, K., Miledi, R., and Stinnakre, J. (1982). Cholinergic and catecholaminergic receptors in the Xenopus oocyte membrane. J. Physiol. *328*, 143–170.

22. Frankenhaeuser, B., and Huxley, A.F. (1964). The action potential in the myelinated nerve fiber of Xenopus laevis as computed on the basis of voltage clamp data. J. Physiol. *171*, 302–315.

23. Sigg, D. (2014). Modeling ion channels: past, present, and future. J. Gen. Physiol. *144*, 7–26.

24. Schwarz, J.R., Reid, G., and Bostock, H. (1995). Action potentials and membrane currents in the human node of Ranvier. Pflugers Arch. *430*, 283–292.

25. The 1000 Genomes Project Consortium (2015). A global reference for human genetic variation. Nature *526*, 68–74.

26. Meyer, M., Kircher, M., Gansauge, M.T., Li, H., Racimo, F., Mallick, S., Schraiber, J.G., Jay, F., Prüfer, K., de Filippo, C., et al. (2012). A high-coverage genome sequence from an archaic Denisovan individual. Science *338*, 222–226.

27. Huerta-Sánchez, E., Jin, X., Asan, Bianba, Z., Peter, B.M., Vinckenbosch, N., Liang, Y., Yi, X., He, M., Somel, M., et al. (2014). Altitude adaptation in Tibetans caused by introgression of Denisovan-like DNA. Nature *512*, 194–197.

28. Dannemann, M., Andrés, A.M., and Kelso, J. (2016). Introgression of Neandertal- and Denisovan-like haplotypes contributes to adaptive variation in human Toll-like receptors. Am. J. Hum. Genet. *98*, 22–33.

29. Kong, A., Gudbjartsson, D.F., Sainz, J., Jonsdottir, G.M., Gudjonsson, S.A., Richardsson, B., Sigurdardottir, S., Barnard, J., Hallbeck, B., Masson, G., et al. (2002). A high-resolution recombination map of the human genome. Nat. Genet. *31*, 241–247.

30. Hasegawa, M., Kishino, H., and Yano, T. (1985). Dating of the human-ape splitting by a molecular clock of mitochondrial DNA. J. Mol. Evol. *22*, 160–174.

31. McLaren, W., Gil, L., Hunt, S.E., Riat, H.S., Ritchie, G.R., Thormann, A., Flicek, P., and Cunningham, F. (2016). The Ensembl variant effect predictor. Genome Biol. *17*, 122.

32. Dannemann, M., Prüfer, K., and Kelso, J. (2017). Functional implications of Neandertal introgression in modern humans. Genome Biol. *18*, 61.

33. GTEx Consortium (2015). Human genomics. The Genotype-Tissue Expression (GTEx) pilot analysis: multitissue gene regulation in humans. Science *348*, 648–660.

34. Cummins, T.R., Rush, A.M., Estacion, M., Dib-Hajj, S.D., and Waxman, S.G. (2009). Voltage-clamp and current-clamp recordings from mammalian DRG neurons. Nat. Protoc. *4*, 1103–1112.

35. Milescu, L.S., Bean, B.P., and Smith, J.C. (2010). Isolation of somatic Na+ currents by selective inactivation of axonal channels with a voltage prepulse. J. Neurosci. *30*, 7740–7748.

CellPress
OPEN ACCESS

STAR★METHODS

KEY RESOURCES TABLE

REAGENT or RESOURCE	SOURCE	IDENTIFIER
Chemicals, Peptides, and Recombinant Proteins		
Normal Frog Ringer	EcoCyte Bioscience	Cat#: 1688
Modified Barths Solution	EcoCyte Bioscience	Cat#: 1697
Penicillin-Streptomycin	Sigma-Aldrich	Cat#: P4333
Sodium pyruvate	Sigma-Aldrich	Cat#: P2256
Dulbecco's modified Eagle medium	Sigma-Aldrich	Cat#: D5796
TrypLE Express Enzyme	Thermo-Fisher	Cat#: 12605010
Fetal Bovine Serum	Sigma-Aldrich	Cat#: F7524
Critical Commercial Assays		
mMESSAGE mMACHINE T7 ULTRA Transcription Kit	Thermo-Fisher	Cat#: AM1345
Deposited Data		
Archaic genomes	Max-Planck Institute EVA	http://cdna.eva.mpg.de/neandertal
1000 genome project	The International Genome Sample Resource	http://www.internationalgenome.org/data
UK BioBank	UK Biobank Limited	https://www.ukbiobank.ac.uk/
GTEx gene expression	The Genotype-Tissue Expression (GTEx) project	https://gtexportal.org/home/datasets
Experimental Models: Organisms/Strains		
Xenopus oocytes	EcoCyte Bioscience	First grade
Human embryonic kidney cells	University of Cambridge	HEK293T
Recombinant DNA		
SCN9A (Nav1.7) cDNA	GenScript	Cat#: OHu22884
SCN3B (Navβ3) cDNA	GenScript	Cat#: OHu16302
pXOOM vector	Søren Olesen [19]	N/A
Software and Algorithms		
MATLAB	MathWorks	R2018a
R	R Foundation	ver. 3.5.3

RESOURCE AVAILABILITY

Lead Contact
Further information and requests for resources and reagents should be directed to and will be fulfilled by the Lead Contact, Hugo Zeberg (hugo.zeberg@ki.se).

Materials Availability
The plasmids encoding the Nav1.7 variants are available from the Lead Contact upon request.

Data and Code Availability
The recording software, utilizing the MATLAB Data Acquisition Toolbox, and electrophysiological data, including steady-state inactivation and activation as a function of voltage, are available at https://gin.g-node.org/hugozeberg/SCN9A. Code used for this study and raw data are available upon request.

EXPERIMENTAL MODEL AND SUBJECT DETAILS

Xenopus laevis (EcoCyte Bioscience, Castrop-Rauxel, Germany) oocytes were kept at 12°C in Modified Barth Solution, supplemented with 2.5 mM sodium pyruvate and 25 U/mL penicillin and 25 μg/ml streptomycin. HEK293T cells were cultured in Dulbecco's Modified Eagle Medium (DMEM), supplemented with 10% fetal calf serum and 100 U/ml penicillin and 0.1 mg/ml streptomycin, at

Current Biology
Report

37°C in a 5% carbon dioxide humidified incubator. For the human phenotypic analysis, 198,047 adult females and 164,897 adult males from United Kingdom were included in the study (the UK Biobank).

METHOD DETAILS

Molecular biology

SCN9A (Nav1.7) and *SCN3B* (Navβ3) cDNAs were synthesized by GenScript (Piscataway, NJ). The *SCN9A* construct used is the most abundant splice isoform in dorsal root ganglia (DRG), and corresponds to the RefSeq sequence NM_002977.3, which encodes a W at position 1150, as in the majority of modern humans, as well as in all three high-coverage Neanderthal genomes. In contrast, the human reference carries an R at this position seen in 13% of present-day humans (rs6746030). pXOOM [19] was used as the plasmid backbone and all constructs were verified by sequencing. Plasmids were linearized with the restriction enzyme *XhoI* and transcribed *in vitro* using the T7 mMessage mMachine ULTRA kit (Ambion, Austin, TX). cRNA concentration and purity were determined using a spectrophotometer.

Oocyte injection

Stage V-VI oocytes injected using a Nanoject II Auto-Nanoliter Injector (Drummond Scientific, Broomall, PA) with 2 ng *SCN9A* cRNA and (in experiments with the Navβ3 subunit) 20 ng *SCN3B* cRNA in a volume of 50 nL RNase-free water. *SCN3B* was injected in excess relative to *SCN9A*, in order to assure that Nav1.7 channels were complexed with Navβ3 subunits. After injection, oocytes were incubated at 12°C for 4-6 days, before electrophysiological recordings.

Transfection of HEK293T cells

HEK293T cells were transfected with 2 μg of each of the two cDNA vectors using 10 μg branched polyethylenimine (~25kDa) in 2 mL of DMEM in 9.5 cm^2 wells for 4 hours. Cells were harvested using TrypLE Express Enzyme, seeded in 3.5 cm dishes, and used for voltage clamp experiments 24-48 hours post transfection.

Voltage clamp recordings in *Xenopus* oocytes

Experiments were performed at 10 ± 2°C using a two-electrode voltage-clamp setup and either a CA-1 amplifier (Dagan, Minneapolis, MN), or an OC-725C amplifier (Warner Instruments, Hamden, CT). Data were acquired at 100 kHz via a NI-6221 DAQ using custom written software in MATLAB (Mathworks, Natick, MA). External solution consisted of (in mM); 90 NaCl, 2 KCl, 1 MgCl$_2$, 2 CaCl$_2$, and 5 HEPES, adjusted to pH 7.2. Micropipettes were pulled from borosilicate glass capillaries (Harvard Apparatus, Holliston, MA) and had a resistance of 0.5-1 MOhm when filled with 3M KCl. The bath potential was actively controlled to minimize series resistance in the bath and across the bath-grounding electrode. Oocytes had an input resistance of 1.6 ± 0.9 MOhm (n = 216).

The voltage clamp protocols are shown in Figure S1A. The first 300 ms pulse from the baseline of −90 mV was used to measure channel activation and the time constant for inactivation. Steady-state inactivation was measured by a second 0 mV pulse immediately following the first pulse, given the temperature coefficient of the fast inactivation (Q10 ~3 [20]), a 300-ms prepulse is equivalent to 100-ms prepulse at room temperature. Membrane potential was clamped at −90 mV for 5 s between consecutive trials. Current traces (Figure S2) were filtered after recordings using a rolling average of 100 data points. In Figure 1A, capacitive transients (time constant of ~1 ms) have been eliminated by fitting and subtracting a single exponential. For data analysis, we measured the current amplitude at t = 10 ms (into the 0-mV step), a time point at which virtually all capacitive transients had declined (~0.004% of the initial stimulation, or ~2 nA, remained). For inactivation measurements, the current following a prepulse to +10 mV was taken as baseline (I$_{base}$; compensating for any non-inactivating currents, including leak currents) and current (I) was normalized to the maximal observed current in that cell (I$_{max}$) according to (I-I$_{base}$)/(I$_{max}$-I$_{base}$). The channels were considered to have fully inactivated following the +10 mV prepulse, based on previous work in *Xenopus* oocytes [14].

Activation as a function of voltage was measured as peak inward current relative to the current observed at the end of the 300 ms into the first pulse (i.e., immediately before the second pulse to 0 mV). Currents were converted to conductance using g = I/(V-E$_{rev}$Na). The reversal potential E$_{rev}$Na was calculated using the Nernst equation, assuming an intracellular sodium concentration of 22.5 mM [21], yielding a reversal potential of +33.8 mV.

Data were fitted to a first (inactivation) or second-order Boltzmann equation (activation; as suggested by the Frankenhaeuser-Huxley model [22]). The curves were fitted over the dynamic range of the functions (−40 to 0 mV for activation and −70 to −10 mV for inactivation). For the activation function, a fixed slope of 5.9/mV provided the overall best fit (see Figures S1D–S1G) and for the steady-state inactivation function, 15.1/mV (Figures S1I–S1L). The numerical values of the fitted midpoint potentials are given in Table S1.

The time-constants for inactivation were measured by fitting a single exponential between 10 and 20 ms into the 300-ms pulse, in traces showing a current decay > 10 nA from 10 to 20 ms. Outliers were detected using the built in outlier detection in MATLAB. Whereas the data points are experimental measurements, the bell-shaped curves in Figures S1O–S1Q are derived using a kinetic model [23] with values from the steady-state inactivation curves.

Voltage clamp experiments in HEK293T cells

HEK293T cells were analyzed at room temperature (~23°C) using either an Axon Multiclamp 700A or a 700B patch-clamp amplifier, Molecular Devices, San Jose, CA. The pXOOM vector encodes an enhanced green fluorescent protein, which was excited to identify transfected cells. The external solution consisted of (in mM); 140 NaCl, 2.5 KCl, 1 MgCl$_2$, 2 CaCl$_2$, 10 glucose, and 10 HEPES, adjusted to pH 7.4 with NaOH. Patch pipette were pulled from borosilicate glass capillaries (Harvard Apparatus, Holliston, MA), and the tip of the electrode was fire-polished. For low noise voltage-clamp recordings (Figure S2) with potassium currents blocked, pipettes were filled with a solution, containing (mM): Cs methane sulfonate 125, CsCl 5, KCl 10, EGTA 1, 10 HEPES, 4 Mg-ATP, 0.3 GTP-Na$_2$, 10 creatine phosphate-Na, pH adjusted to 7.3 with CsOH. Electrodes had a resistance of 4-11 MΩ, and the membrane potential signal was corrected for nulling of the liquid junction potential before seal formation. Data was filtered using a low-pass filter at 6 kHz (Bessel, 8-pole) and sampled at 20 kHz via a NI-X-series DAQ using custom software written in MATLAB (Mathworks, Natick, MA). Recording pipettes were positioned with LM-Mini stepper-motor-controlled micromanipulators (Luigs and Neumann, Ratingen, Germany). Cells had an input resistance of 1.5 ± 1.6 GOhm (min = 112 Mohm, max = 4.5GOhm, n = 17). A P/n protocol consisting of 4 negative steps in every sweep, each 5 mV and 500 ms long, was used to compensate for passive membrane properties. Capacitance was also compensated for by the built-in capacitance correction circuit of the amplifier. In order to adjust for the effect of nonlinearity in the background current, the P/n correction was scaled to between 30% and 100% to minimize the amplitude of the residual capacitance transient. The leak conductance was estimated using the current response between −120 to −70 mV, before any activation of the Na current.

Activation and inactivation were investigated with the voltage clamp protocol shown in Figure S1A. Amplitude was measured as the peak inward current. Given that inactivation is hyperpolarized in mammalian cells, the voltage protocol spanned the range −120 mV to +10 mV. Activation of conductance as a function of voltage was computed using the sodium equilibrium potential of +65mV. Data were fitted over the entire range to a first (inactivation) or second-order Boltzmann equation (Figures S1C and S1H). The slopes from the oocyte experiments provided a good fit for HEK cells and were kept as fixed constants. The numerical values of the fitted midpoint potentials are given in Table S1.

Computational modeling

The effect of a 10-mV shift of activation and fast inactivation was studied using a model of a peripheral nerve, based on voltage clamp data from the human node of Ranvier [24] (ModelDB; accession: 261436). The model was implemented in MATLAB.

Amino-acid substitutions in Neanderthal ion channels

Fifteen voltage gated-like ion channels (CACNA1D, CACNA1H, CACNA1S, CATSPER3, CNGB1, HCN4, KCNH3, KCNK2, KCNV2, PKD2L, SCN9A, TRPC6, TRPM1, TRPM4, and TRPV4) carry amino-acids substitutions in the three high-coverage Neanderthal genomes available. Expression data of these 15 channels in single-cell RNA sequencing data from rodent DRG [7] showed high expression of *SCN9A* only.

Archaic introgression

Potentially introgressed segments in and around *SCN9A* were identified by studying "archaic single-nucleotide polymorphisms" ("aSNPs") defined as those that are homozygous ancestral in all 1,000G (phase III) Yoruba individuals [25], homozygous derived in at least one of the Altai Neanderthal, the Vindija Neanderthal, and the Denisovan genomes [2, 6, 26], and for which the derived allele is present in at least one non-African 1,000G individual. In addition, aSNPs were required to overlap previously identified regions of Neanderthal introgression in present-day humans, *i.e.*, having a Neanderthal posterior probability greater than 0.9 and a length of at least 0.02 cM [3].

The likelihood of incomplete lineage sorting was tested using a published method [27], an age of the Altai Neanderthal based on a mutation rate of 1.0x10^{-9} per base pair per year [28], and the local recombination rate estimate [29].

The relationships of present-day and Neanderthal DNA segments were estimated using genotype information from 1,000G (phase III) individuals, excluding sites that were missing in at least one individual or were heterozygous in one of the three archaic individuals. This resulted in 727 variable positions in the regions overlapping V991L and M932L, and 2,868 variable sites in the region overlapping D1908G. Haplotypes that had less than five differences per 10,000 base pairs to each other were clustered, resulting in six clusters per region. Consensus sequences were generated by randomly selecting a variant at each position. Based on 100 and 363 positions that were variable among these consensus sequences, maximum-likelihood phylogenies were constructed using the Hasegawa-Kishino-Yano-85 model [30] with a proportion of invariable sites and a discrete-gamma distribution to account for variable substitution rates among sites.

Phenotypic consequences of Nav1.7 variants

Excluding individuals that were related, showed unusually low levels of heterozygosity, or who had substantial non-British ancestry left 362,944 of 487,409 individuals from the UK Biobank [18], which were used for subsequent analysis. All combinations of the three variants were tested for correlations with the 19 pain phenotypes and additionally with a composite binary measure that reflects whether an individual was positive for at least one of the 19 pain-related phenotypes (Table S3). Correlations between genotypes and pain phenotypes were assessed using logistic regression, including sex and age as co-factors in the linear model. Whereas the primary analysis involving the composite pain measure for the Neanderthal Nav1.7 variant rejected the null hypothesis, none

Current Biology
Report

of the other secondary analyses resulted in a p value < 0.05, and hence these p values were not adjusted for multiple comparisons. The potential impact of noncoding aSNPs was identified using the Variant Effect Predictor [31, 32]. Identified noncoding variants were then checked for expression changes in 48 GTEx tissues [33].

QUANTIFICATION AND STATISTICAL ANALYSIS

Oocytes were randomly selected for injection of different mRNA transcripts. Each oocyte was used only once (n = 216). HEK cells were selected based on expression of GFP (n = 17). For the electrophysiology recordings, data were collected until the SEM of the midpoint potentials of the steady-state activation and inactivation curves were less than ± 1.5mV. Recordings from oocytes that had a holding current greater than 5 μA at −90mV were excluded. HEK cells were excluded if they had a leak current larger than 500 pA at −120mV, did not display a Na current (an inward current at −20mV with a peak around 1-2 ms), displayed other inward ion current fractions, or showed an atypical current-voltage relationship [34, 35] due to suboptimal recording conditions (sum of square errors > 0.05 of the fit of a standard first-order Boltzmann curve to the inactivation process). The significance of any difference in the midpoint potentials was determined using a two-tailed t test with n-2 degrees of freedom, corrected for multiple comparisons using Bonferroni correction. The normality of midpoint potentials was verified using the Shapiro-Wilk test.

ADDITIONAL RESOURCES

The archaic genomes are available at http://cdna.eva.mpg.de/neandertal/. The genomes from the 1000 Genomes Project are available at http://www.internationalgenome.org/data. The UK BioBank is available at https://www.ukbiobank.ac.uk/. GTEx gene expression data is available at https://gtexportal.org/home/datasets.

Supplemental Information

A Neanderthal Sodium Channel Increases

Pain Sensitivity in Present-Day Humans

Hugo Zeberg, Michael Dannemann, Kristoffer Sahlholm, Kristin Tsuo, Tomislav Maricic, Victor Wiebe, Wulf Hevers, Hugh P.C. Robinson, Janet Kelso, and Svante Pääbo
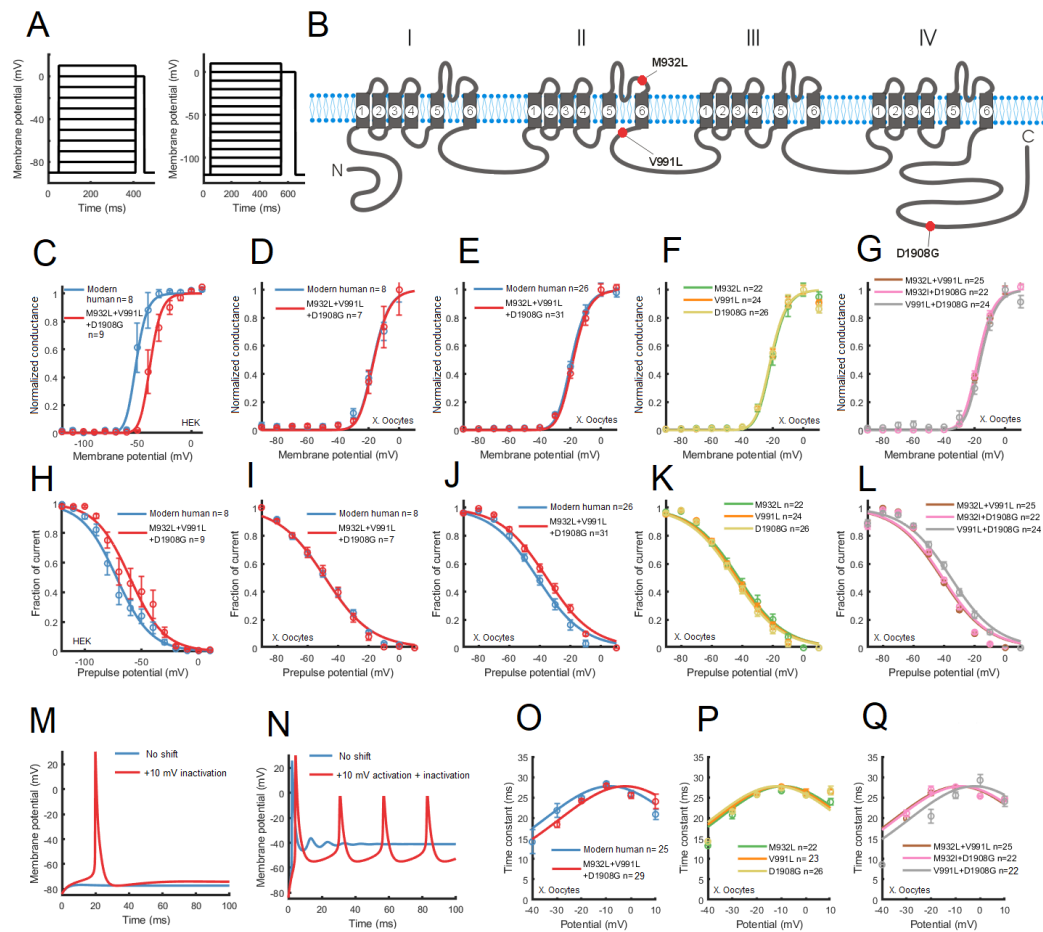
Figure S1. Effects of Neandertal-derived amino acid substitutions on Nav1.7 activation and steady-state inactivation. Related to Figure 1. A) Protocols used for voltage clamp on *Xenopus* oocytes (left) and HEK cells (right). Cells were clamped for 5 s at -90 mV (oocytes) or -120 mV (HEK cells) between sweeps. Each sweep consisted of longer step, incremented by 10 mV, followed by shorter step to 0 mV, as shown in the figure. **B**) Schematic of the Nav1.7 protein, showing the positions of the Neandertal-derived amino-acid substitutions. **C**) Activation functions for the modern human- and Neandertal versions of Nav1.7, co-expressed with the beta subunit, Navβ3, when expressed in HEK 293T cells. For the Neandertal Nav1.7, activation is shifted by ~12 mV to more depolarized potentials. **D**) Activation functions for the modern human- and Neandertal versions of Nav1.7 in the absence of the beta subunits in *Xenopus* oocytes, **E-G**) Activation functions for Nav1.7 when co-expressed with the beta subunit, Navβ3, in *Xenopus* oocytes. Functions are shown for Nav1.7 as found in modern humans, and with the Neandertal-derived amino-acid substitutions singly, and in combinations of two and three, as indicated. **H**) Inactivation functions for the modern human- and Neandertal versions of Nav1.7, co-expressed with the beta subunit, Navβ3, when expressed in HEK 293T cells. For the Neandertal Nav1.7, inactivation is shifted by ~12 mV to more depolarized potentials. **I**) Inactivation functions for the modern human- and Neandertal versions of Nav1.7 in the absence of beta subunits in *Xenopus* oocytes. **J-L**) Inactivation functions for Nav1.7 when co-expressed with the beta subunit, Navβ3, in *Xenopus* oocytes. Functions are shown for Nav1.7 as found in modern humans, and with the Neandertal-derived amino-acid substitutions singly, and in combinations of two and three, as indicated. Navβ3 co-expression shifts the inactivation function by ~7 mV to more depolarized potentials, with an additional depolarizing shift of ~6 mV for M932L+V991L+D1908G and V991L+D1908G. **M**) Voltage trajectories for a computational model of a human peripheral nerve. A depolarising shift in inactivation lowers the threshold and results in an action potential when stimulated with $5\mu A/cm^2$. **N**) A depolarising shift in both activation and inactivation results in repetitive firing when stimulated with $26\mu A/cm^2$. **O-Q**) Inactivation time constants in the presence of Navβ3. Error bars represent S.E.M.
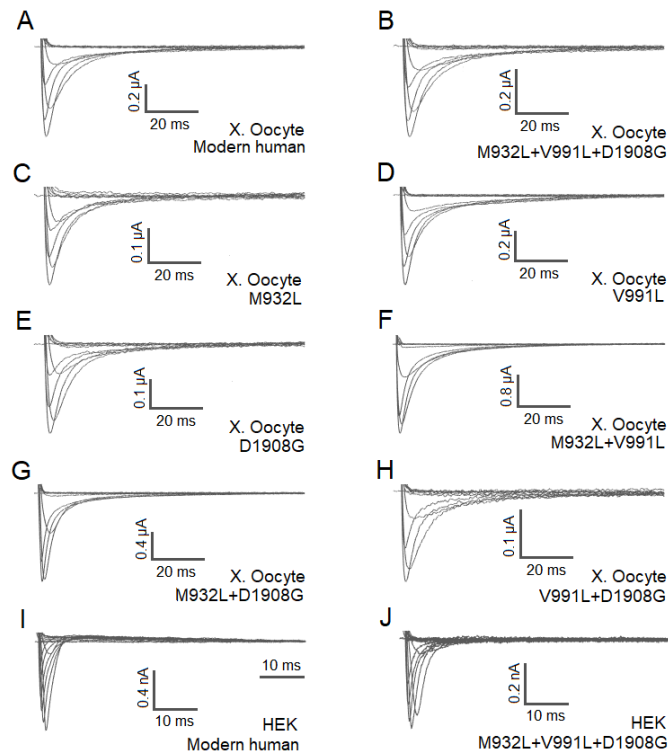
Figure S2. Families of current traces of cells expressing the modern Nav1.7 channel and various combinations of the Neandertal amino acid substitutitons. Related to Figure 1. A-H) Current traces from voltage-clamp experiments in *Xenopus* oocytes (first 100 ms of the protocol). Peak inward-current amplitude: 0.2-2.2 μA. **I-J**) Current traces from voltage-clamp experiments in HEK-293T cells (first 60 ms of the protocol). Peak inward-current amplitude: 0.5-1.0 nA.
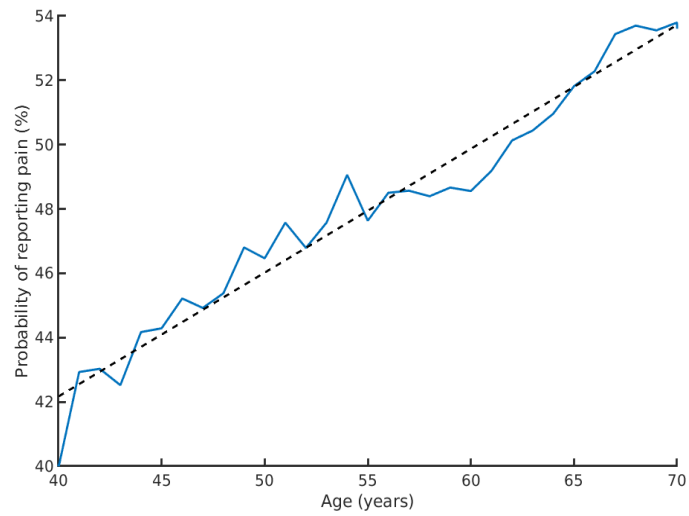
Figure S3. Probability of reporting pain in the UK Biobank as a function of age. **Related to Figure 3.** Linear regression with a slope of 0.39% per year shown as dashed line. From the slope of the linear regression, the effect size of having the Neandertal Nav1.7 variant corresponds to an increase in the probability of reporting pain of approximately 8 years and 6 months of "additional" age. Controlling for the covariates, *i.e.* using the quotients of the coefficients in the logistic regression, yields 9 years and 9 months.

	Activation			Inactivation		
	$V_{1/2}\pm$s.e.m.(mV)	Δ	p-value	$V_{1/2}\pm$s.e.m.(mV)	Δ	p-value
Xenopus oocytes						
Modern human	-22.1 ± 0.79			-48.37 ± 0.48		
M932L+V991L+D1908G	-21.8 ± 1.49	0.30	1.00	-48.46 ± 0.78	0.09	1.00
Co-expressed with Navβ3						
Modern human	-24.46 ± 1.00			-41.68 ± 0.89		
M932L+V991L+D1908G	-23.36 ± 0.92	1.10	1.00	-35.54 ± 0.72	**6.14**	0.00
M932L	-26.16 ± 1.30	-1.69	1.00	-42.42 ± 1.05	-0.74	1.00
V991L	-26.69 ± 0.66	-2.23	0.13	-43.71 ± 0.71	-2.03	1.00
D1908G	-26.72 ± 0.89	-2.26	0.26	-45.06 ± 0.76	-3.38	0.10
M932L+V991L	-22.61 ± 0.68	1.86	0.46	-41.65 ± 0.50	0.03	1.00
M932L+D1908G	-23.10 ± 0.64	1.36	1.00	-40.84 ± 0.61	0.85	1.00
V991L+D1908G	-21.40 ± 1.31	3.06	0.14	-35.54 ± 0.67	**6.15**	0.00
HEK 293T						
Co-expressed with Navβ3						
Modern human	-56.34 ± 1.73			-72.08 ± 1.39		
M932L+V991L+D1908G	-43.10 ± 1.69	**13.24**	0.00	-60.40 ± 2.26	**11.68**	0.01

Table S1. Midpoint potentials for activation and inactivation functions. Related to Figure 1. The shifts relative to the modern human Nav1.7 channel are shown in the Δ-columns. Note, that since activation was fitted to a squared Boltzmann function, $V_{1/2}$ corresponds to an activation of 0.25 (*i.e.*, the midpoint potential refers to the activation state of a single gate in the protein). Significant shifts are bold.

	M932L	V991L	D1908G	M932L+V991L +D1908G
East Asia				
CHB	7.8	7.8	10.2	4.9
JPT	4.8	4.8	9.1	3.8
CHS	5.1	5.1	17.1	4.7
CDX	5.6	5.6	16.7	4.3
KHV	6.9	6.9	14.4	4.5
South Asia				
GIH	0.9	0.9	0	0
PJL	1.6	1.6	0	0
BEB	1.2	1.2	2.3	1.2
STU	1.9	1.9	0.5	0
ITU	1.0	1.0	0	0
Europe				
CEU	0	0	0	0
TSI	0	0	0	0
FIN	0	0	0	0
GBR	0	0	0	0
IBS	0	0	0	0
Africa				
YRI	0	0	0	0
LWK	0	0	0	0
GWD	0	0	0	0
MSL	0	0	0	0
ESN	0	0	0	0
America				
ASW	2.3	2.3	2.3	1.6
ACB	0.5	0.5	0.5	0.5
MXL	22.4	22.4	32.1	18.0
PUR	3.8	3.8	9.0	2.9
CLM	5.3	5.3	16.5	4.3
PEL	23.8	23.3	52.9	21.8

Table S2. Frequencies of the three Neandertal-derived amino-acid substitutions in 1000G populations (%). Related to Figure 2. CHB, Han Chinese in Beijing; JPT, Japanese in Tokyo; CHS, Southern Han Chinese; CDX, Chinese Dai in Xishuangbanna; KHV, Kinh in Ho Chi Minh City; GIH, Gujarati Indian from Houston, Texas; PJL, Punjabi from Lahore; BEB, Bengali from Bangladesh; STU, Sri Lankan Tamil from the UK; ITU, Indian Telugu from the UK; CEU, Utah Residents with Northern and Western European Ancestry; TSI, Toscani in Italia; FIN, Finnish in Finland; GBR, British in England and Scotland; IBS Iberian Population in Spain; YRI, Yoruba in Ibadan; LWK, Luhya in Webuye; GWD, Gambian in Western Divisions; MSL, Mende in Sierra Leone; ESN, Esan in Nigeria; ASW, Americans of African Ancestry in SW USA; ACB, African Caribbeans in Barbados; MXL, Mexican Ancestry from Los Angeles; PUR, Puerto Ricans; CLM, Colombians from Medellin; PEL, Peruvians from Lima.
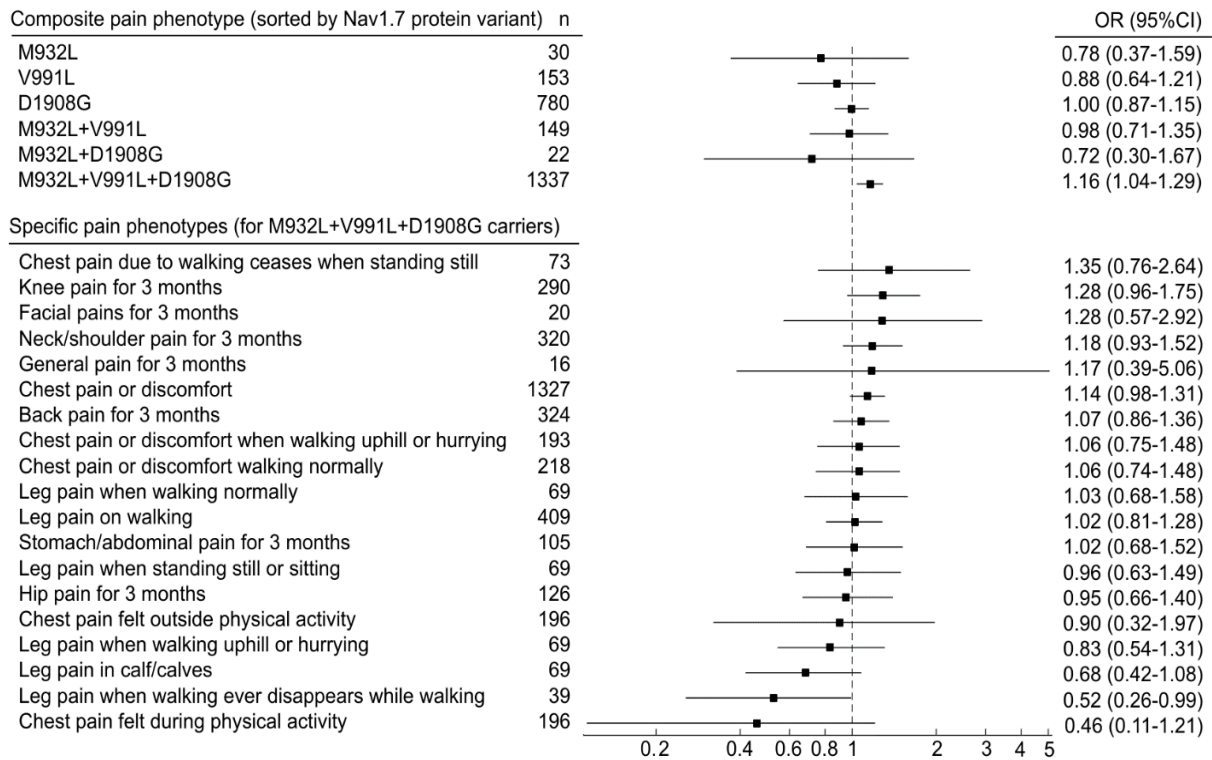
Composite pain phenotype (sorted by Nav1.7 protein variant)	n	OR (95%CI)
M932L	30	0.78 (0.37-1.59)
V991L	153	0.88 (0.64-1.21)
D1908G	780	1.00 (0.87-1.15)
M932L+V991L	149	0.98 (0.71-1.35)
M932L+D1908G	22	0.72 (0.30-1.67)
M932L+V991L+D1908G	1337	1.16 (1.04-1.29)

Specific pain phenotypes (for M932L+V991L+D1908G carriers)	n	OR (95%CI)
Chest pain due to walking ceases when standing still	73	1.35 (0.76-2.64)
Knee pain for 3 months	290	1.28 (0.96-1.75)
Facial pains for 3 months	20	1.28 (0.57-2.92)
Neck/shoulder pain for 3 months	320	1.18 (0.93-1.52)
General pain for 3 months	16	1.17 (0.39-5.06)
Chest pain or discomfort	1327	1.14 (0.98-1.31)
Back pain for 3 months	324	1.07 (0.86-1.36)
Chest pain or discomfort when walking uphill or hurrying	193	1.06 (0.75-1.48)
Chest pain or discomfort walking normally	218	1.06 (0.74-1.48)
Leg pain when walking normally	69	1.03 (0.68-1.58)
Leg pain on walking	409	1.02 (0.81-1.28)
Stomach/abdominal pain for 3 months	105	1.02 (0.68-1.52)
Leg pain when standing still or sitting	69	0.96 (0.63-1.49)
Hip pain for 3 months	126	0.95 (0.66-1.40)
Chest pain felt outside physical activity	196	0.90 (0.32-1.97)
Leg pain when walking uphill or hurrying	69	0.83 (0.54-1.31)
Leg pain in calf/calves	69	0.68 (0.42-1.08)
Leg pain when walking ever disappears while walking	39	0.52 (0.26-0.99)
Chest pain felt during physical activity	196	0.46 (0.11-1.21)

(x-axis: 0.2 0.4 0.6 0.8 1 2 3 4 5)

Table S3. Odds ratios for experiencing pain in individuals from the UK Biobank. Related to Figure 3. Above, odds ratios for the composite pain phenotype (positive for any of the 19 specific pain phenotypes), by Nav1.7 protein variant. Below, odds ratios for 19 specific pain phenotypes in carriers of the Neandertal-like Nav1.7 protein (M932L+V991L+D1908G). Horizontal lines indicate 95% confidence intervals.